ACS APPLIED MATERIALS & INTERFACES

RESEARCH ARTICLE

www.acsami.org

Structure, Sodium Ion Role, and Practical Issues for β-alumina as a High-*k* Solution-Processed Gate Layer for Transparent and Low-Voltage Electronics

Bo Zhang, Yu Liu, Shweta Agarwal, Ming-Ling Yeh, and Howard E. Katz*

Department of Materials Science and Engineering, Johns Hopkins University, 206 Maryland Hall, 3400 North Charles Street, Baltimore, Maryland 21218, United States

ABSTRACT: Sodium β-alumina (SBA)-based gate dielectric films have been developed for all solution-processed, transparent and low voltage field-effect transistors (FETs). Its high dielectric constant has been ascribed to sodium (Na+) ions in the crystal structure; however, there are no published experimental results concerning the contribution of Na+ ions to the dielectric behavior, and the degree of crystallinity of the thin films. In addition, as an ionic conductor, β-alumina could give rise to some issues such as leakage current caused by Na diffusion, threshold voltage shift due to interface charge accumulation and longer response time due to slower polarization of the Na+ ions. This paper will address these issues using zinc tin oxide (ZTO) FETs, and propose possible measures to further improve SBA-based gate materials for electronic devices.

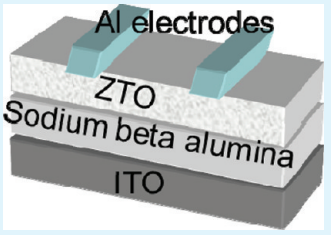

KEYWORDS: sodium beta-alumina, dielectric, low voltage, transparent electronic, oxide semiconductor, and transistor

INTRODUCTION

In the past two decades, considerable efforts have been devoted to the development of organic, polymer, and ZnO-based semiconductor layers for printable, low-cost, macrosized transistors that can be integrated into transparent, flexible electronic devices such as electronic book readers, flat panel TVs and so forth.[1−8] However, the present disadvantage for these materials as compared to silicon wafer technology is the 2−3 orders of magnitude lower mobility. As a result, a high gate voltage, e.g., >30 V, has to be applied to these devices (e.g., if using 100 nm SiO_2 as gate) to drive usable source-drain currents, which significantly limits the development of commercial components from these semiconductor materials. To reduce the operational voltage, one may enhance the mobility of these materials; another alternative is to develop high dielectric constant material (high-*k* material) as a gate layer, which allows more carriers to be induced at a lower voltage.

A high-*k* material allows the gate film to achieve a desired high capacitance with larger thickness. Thicker films can help reduce the leakage current arising from structural defects and carrier tunneling. However, some high k materials are unsuitable for gate layers in FETs[9] because of one or more of the following: (1) formation of polycrystalline films rather than glasses. Crystallization will give rise to grain boundaries at which leakage current is concentrated. One of the advantages of the SiO_2 gate is that it maintains at an amorphous state up to 1100 °C. Many high-*k* oxides have low crystallization temperature which prevents them from being used as gate materials.[10] The candidate to replace SiO_2 in silicon technology, HfO_2, has crystallization temperature above 900 °C. (2) Insufficient band offset with semiconductor layers. A small band gap offset will result in leakage current by charge injection and give rise to hot-carrier emission. SiO_2 has a band gap as large as 8.9 eV. (3) Thermal and chemical instability in the presence of the semiconductor layer, for example leading to oxidation or diffusion phenomena. (4) Surface defects leading to operational instability of FETs. One advantage of SiO_2 is the small defect density due to its high process temperature, and covalent bonds with low coordination which allow any dangling bonds to self-heal back to the network. In contrast, many other ionic bonding oxides such as Al_2O_3, HfO_2, and ZrO_2 have higher defect concentrations.

In 2009, our group reported a high k material, sodium-doped beta-alumina (SBA).[11] The sol−gel derived thin film (75 nm) possesses a dielectric constant (k) up to 170, which is much higher than traditionally used SiO_2, with k = 3.9, and other possible alternatives to SiO_2, such as ZrO_2, k = 23, and HfO_2, k = 20. The zinc tin oxide (ZTO) FETs made by using this SBA gate layer can output hundreds of microamperes with an operational voltage of 2 V, a significantly lower voltage than the same ZTO device using SiO_2 as gate layers (30 V for 100 nm SiO_2). The mechanism behind this high dielectric constant of SBA was thought to come from its crystal structure. SBA originally attracted much attention due to its high ionic conductivity, of great of importance for solid-state electrolytes. SBA has a layered crystal structure in which loosely bonded Na+ ions are sandwiched by two spinel blocks made of Al and O atoms, so in the ab plane the Na+ ions can move easily giving a good electrical conductivity. However, in the c direction, the movement of

Received: July 11, 2011
Accepted: October 6, 2011
Published: October 06, 2011

dx.doi.org/10.1021/am2009103 | *ACS Appl. Mater. Interfaces* 2011, 3, 4254–4261

Na+ ions is confined by the spinel blocks. Using aforementioned criteria to review SBA, we found that (1) SBA is a moderate glass former. The SBA materials we study here have nominal bulk crystallization temperatures of 720 and 830 °C based on powder samples. (2) The band gap is large; SBA along the *c* axis has a band gap of 8.8 eV, comparable to 8.9 eV of SiO_2, and much larger than other oxide gate material candidates, such as HfO_2, band gap 5.6 eV, ZrO_2, band gap 4.7−5.7 eV. (3) SBA has good chemical stability in the presence of popular semiconductor oxides such as indium tin oxide and zinc tin oxide up to 600 °C based on our experiments. (4) The chemistry of SBA allows routes to possible defect passivation, though intrinsically it shares the defect challenges of other oxide dielectrics. In this paper, we address these issues to give clear and comprehensive evaluation of SBA as gate layer material in electronic devices, and further optimization measures will be proposed.

EXPERIMENTAL SECTION

Na−Al_2O_3 and Al_2O_3 sol gel solutions are made based on Yoldas's paper.[12] For SBA, sodium acetate (0.041 g) was dissolved in 50 mL of water and heated to 90 °C. $Al(OC_4H_9)_3$ (1.41 mL) was heated at 90 °C with vigorous stirring. The sodium acetate solution (for SBA) at 90 °C was added, and the temperature was increased to 95 °C with stirring for 0.5 h to form AlO(OH) precipitates. 5 mL of dilute mixed acid (0.2N HNO_3 and 0.2N HCl, 1:1 ratio) was used for peptization. The sol was kept under continuous stirring at 95 °C for 0.5 h and then heated further to 110 °C to boil off water. With 10 mL of water removal, the sol approached the gel point. The clear gel was then filtered through a syringe filter (0.45 μm) and coated over ITO-coated glass (Corning Boro-Aluminosilicate Glass with 30 nm ITO coating supplied by Delta Technologies Limited, part number CB-90IN-1,105). This process was repeated three times. This gel-derived glass layer was heated starting from 350 °C, ramping the temperature to 830 °C. When the temperature of the furnace reached 830 °C, it was immediately turned off. Once the furnace cooled to 600 °C, the samples were removed.

A solution-processed transparent ZTO semiconductor could be solution-deposited over SBA or alumina-coated ITO glass substrates: $ZnCl_2$ (0.05 M) and $SnCl_2$ (0.05 M) were dissolved in 25 mL 2-methoxyethanol solvent with ultrasonication. The substrate was dip-coated with this solution at 2 mm/s with an angle 60° to the horizontal and immediately placed on a 75 °C hot plate. This process was repeated four times. The coated substrate was inserted into a preheated 600 °C furnace and kept for 15 min to form a thin layer of continuous polycrystalline ZTO, 60 nm thick as confirmed by SEM.

An alternative way to coat SBA on ITO glass is to use spin-coating. 4.68 g $Al(NO_3)_3 \cdot 9H_2O$ and 0.11 g sodium bisulfate (for SBA) with 11:1 molar ratio are dissolved into 25 mL of methoxyethanol. The same number of moles of acetylacetone as Al ions is added into the solution as stabilizer and the mixed solution is kept under stirring for 6 h. The solution is filtered through a 0.45 μm PTFE filter and spin coated on the cleaned ITO glass. First, the solution is spin-coated at low speed (500 rpm) for 6 s and then the spin speed is accelerated to 3000 rpm within 3 s and kept at 3000 rpm for 30s. One time spin-coating results in a film thickness of 41.5 nm, measured by profilometry. The coated glass goes through the same annealing process as the dipcoating method. Then the whole process is repeated once to achieve desired thickness about 80 nm. ZTO film also can be spin-coated onto this SBA or alumina layer. 0.3 M ZTO solution for spin coating can be made by mixing $Zn(acetate) \cdot 2H_2O$ and $SnCl_2$ at 1:1 ratio in methoxyethanol with acetylacetone having the same concentration as the total of the Zn and Sn ion concentrations. Aluminum electrodes (100 nm thick) were deposited in a vacuum evaporator using a slim-bar transmission electron microscopy grid (200 mesh) as a shadow mask.

A Dimension 3100 atomic force microscope (AFM) (Bruker Nano, Santa Barbara, CA) was used for the measurements. The contact mode images were obtained using Si_3N_4 contact mode tips (Model DNP) with a nominal spring constant of 0.12 N/m. A scan rate of 2 Hz was used to obtain images (2 × 2) μm to (10 × 10) μm. Representative scans are shown. The scans were filtered using a first order plane fit to the data. The first order plane fit centers the data and removes the tilt from each scan line. Root-mean-square (rms) values were obtained from a (2 × 2) μm scan. The rms is a standard deviation of the z values and is calculated as rms = $(\Sigma(z_i)^2/N)^{1/2}$, where z_i is the current height value and N is the number of points within the (2 × 2) μm square. The average value of multiple rms measurements is reported. The high resolution transmission electron microscopy (HRTEM) picture is taken by a Philips CM 300 FEG transmission electron microscope (field emission gun operating at 297 kV). The X-ray diffraction, using the configuration typical for grazing incidence small-angle X-ray scattering (GISAXS), was carried out at Beamline X13B at the National Synchrotron Light Source at Brookhaven National Laboratories. The in-vacuum undulator was set at minimum gap to give a peak photon flux at a photon energy of 11.45 keV. The incident angle was adjusted to be below the critical angle, and consequently the slits that defined to be 100 μm square, in order to keep the beam restricted to the surface area of the film, thus enhancing the signal-to-noise. A Princeton Instruments CCD area detector was placed 142 mm downstream of the sample. The CCD images were 2084 × 2084 with a pixel spacing of 55 μm. The distance from sample to detector was calibrated with using a NIST standard Al_2O_3 powder. Using this calibration, the observed powder rings were consistent with indium tin oxide. The Aluminum electrodes of the transistor devices (100 nm thick) were deposited in a vacuum evaporator using a slim-bar transmission electron microscopy grid (200 mesh) as a shadow mask. The width and length of the channel is about 100 to 10 μm.

RESULTS AND DISCUSSION

Comparison between Al_2O_3 and SBA as Gate Dielectrics. As a high-*k* material, alumina is a popular choice for FET gate material. There have been many reports of alumina as the gate for electronic display application.[13,14] However, most utilize atomic layer deposition to fabricate the alumina gate, and of course, the resulting films lack the sodium ions. Historically, SBA was thought to be just Na-contaminated alumina.[15] We performed a parallel study of the dip-coated sol−gel alumina and SBA to determine the role of Na+ in the dielectric properties of SBA. Herein we fabricated SBA and Al_2O_3 thin film with similar thickness (Al_2O_3 is 90 nm thick and SBA is about 80 nm thick) as the gate materials using the ZTO layer made by dipcoating for FETs. The process of making Al_2O_3 layer is the same as the SBA including annealing temperature profile except no sodium acetate is added in the sol−gel forming process.

From the output curve shown in Figure 1, it is demonstrated clearly that the Al_2O_3 FET is operated at around 5 V with maximum output current around 0.11 mA, whereas the SBA FET has operational voltage around 2 V and the output current is 4−5 times larger than for Al_2O_3 devices. The ability of SBA to reduce operational voltage is evidently demonstrated. ZTO/SBA devices show better field driven mobility value, 18 $cm^2/(V\,s)$, than ZTO/Al_2O_3, 10 $cm^2/(V\,s)$. Field driven mobility is often cited as one of the most important metrics for the device performance. Mobilities of 10 and 18 $cm^2/(V\,s)$ are comparable to the highest reported values for ZTO/SiO_2 FETs. The on/off ratios of the two devices are similar, around 10^4. Since we use the same dipcoating technique to fabricate the ZTO layer on both alumina and SBA, the film qualities should be comparable, and FET

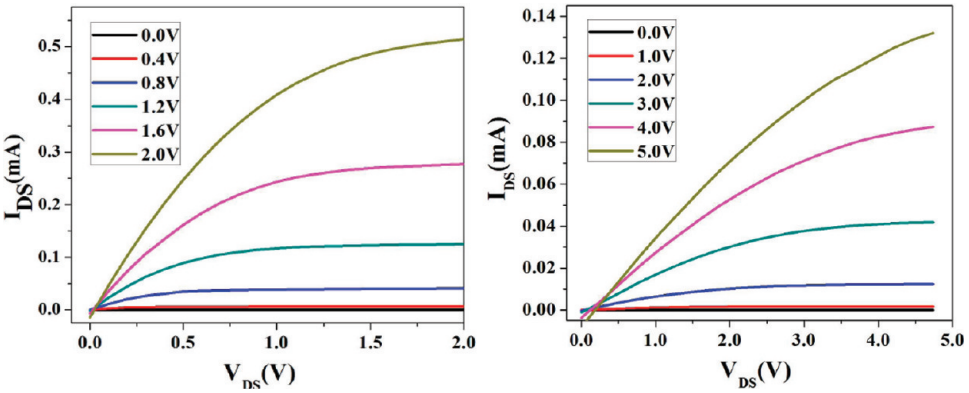

Figure 1. Comparison of output curve of ZTO/SBA (left) and ZTO/Al_2O_3 (right) devices (80 nm SBA, 90 nm Al_2O_3, and W/L ratio = 10). Insets show gate voltages.

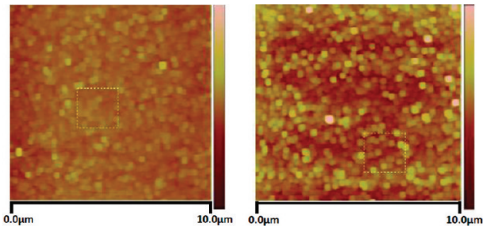

Figure 2. AFM picture of SBA (left) and Al_2O_3 (right) gate layer. The squared-off feature edges are an artifact of the scanning direction.

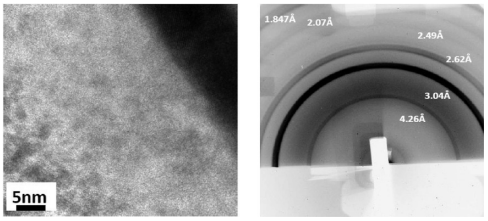

Figure 3. High-resolution transmission electron microscopy picture for SBA−ITO interface (left) and grazing incidence X-ray scattering(right).

performance differences would then be caused by the different dielectric layers. While high capacitance can lower mobility because of increased scattering at the dielectric interface, this is not a universal rule[16,17] and may apply only to semiconductors with the least number of scattering sites otherwise. AFM images, shown in Figure 2, indicate that SBA has lower roughness than Al_2O_3 films. The average roughness for SBA film is 1.15 nm and the one for Al_2O_3 is 1.65 nm. We suggest that the roughness difference can be a factor in the mobility difference between the two types of devices. The possible reason for Al_2O_3 having higher roughness is that the SBA has higher crystallization temperature, one is 720C and the other one is 830C according to.[18] For Al_2O_3, the γ phase and δ phase start to crystallize at 380 and 520 °C based on a previous report.[19] The higher crystallization temperature of SBA leads to less crystallinity than Al_2O_3 under the same annealing temperature profile; consequently giving a smoother surface. From this perspective, the SBA is better glass former than Al_2O_3 in terms of surface roughness, a conclusion that was not anticipated in our earlier work.

TEM images, shown in Figure 3 (left image), offer no sign of long-range crystalline ordering in our SBA film. Grazing-incidence small-angle X-ray scattering (GISAXS), discussed in more detail below, showed peaks assigned to the ITO substrate, and no other peaks. However, the comparison of ZTO/SBA and ZTO/Al_2O_3 devices shown in Figure 1 provides strong support for the statement that SBA film still has a much larger dielectric constant than Al_2O_3 even if it is less crystalline than previously thought. The absolute off-current of SBA/ZTO device is around 1 μA which is higher than the 0.07 μA. However, the on/off ratio for SBA/ZTO is 0.15×10^4 which is slightly less than the one, 0.23×10^4, of Al_2O_3/ZTO. There is no significant on/off ratio decrease by using SBA as dielectric layer. As for the hysteresis, our previous data published in ref 11 have demonstrated that there is no obvious hysteresis for the SBA/ZTO device.

One concern for SBA as gate dielectric was that as an ionic conductor, Na+ ions could move through the SBA causing large gate leakage current. Based on our observations, SBA/ZTO devices do not show higher leakage current than Al_2O_3 (I_g = 4.86 μA at 2 V Vg for SBA device and 5.23 μA for Al_2O_3 device). The small leakage in SBA films is more likely caused by structural defects such as pinholes in the film, rather than Na+ ion motion. This Ig that we do observe is quite stable and does not show a trend of diminishing under operation. If Na caused the leakage current, when Na ions were depleted, we should have seen the leakage current diminishing with longer operational time. We thus conclude that leakage currents are largely electronic, not ionic.

Structure of SBA Film. In our previous paper,[11] we claim the 75 nm SBA film annealed at 830 °C is crystallized. This statement is based on our annealing experiment for SBA powder samples. Clearly, XRD peaks of SBA powder samples annealed at 830 °C indicated crystallinity. At that time, we had not yet obtained XRD diffraction data for thin film samples due to the limitations of on-site instruments. Our more recent experiments suggest that the thin film may still be in an amorphous state that actually favors use as a gate dielectric material. FIB (focused ion beam) is used to cut a thin slice of the SBA film for TEM observation. The gallium ion beam of FIB is perpendicular to the 80 nm thick SBA thin film. The slice thickness is 50 nm. TEM picture showed the cross section of the SBA layer on top of ITO layer. As mentioned above, Figure 3 (left image) shows a TEM image of the thin slice of SBA. The dark region is from ITO coating. Because indium and tin are much heavier elements than Al, the ITO film shows dark color and SBA shows lighter color. From the TEM picture, we can see clear lattice fringes from the ITO region, an indication

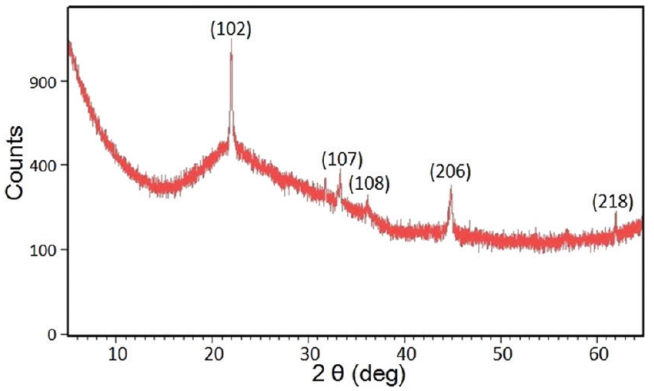

Figure 4. XRD pattern for SBA 90 nm spin coated thin film after annealing at 1000 °C for 15 h.

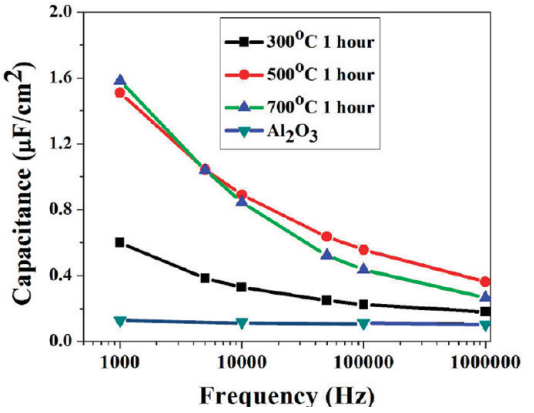

Figure 5. Frequency-dependent capacitance measurements for 90 nm Al_2O_3 and 80 nm SBA thin films annealed at different temperatures.

of crystallization; however, the whole SBA region only shows an amorphous state morphology. We further did grazing incidence X-ray scattering for the SBA samples to confirm the structure of the SBA film. The GISAXS pattern is shown in Figure 3(right image). The rings in the GISAXS pattern correspond to polycrystalline materials. After calculating the crystal plane distance, the *d* spacings are 4.26, 3.04, 2.62, 2.49, 2.23, 2.07, and 1.847 Å, which all correspond to ITO but not SBA. These two experiments consistently show that the SBA layer is still in the amorphous state and ITO is crystallized during annealing. The original ITO coating is amorphous according to the information provided by Delta technology, Inc. It is understandable that the thin film has slightly higher crystallization temperature than its bulk material counterpart because kinetically, the bulk material may have more nucleation sites, and thermodynamically, the thin film has less negative crystallization enthalpy because of the higher fraction of surface atoms. This discovery of the structure of the SBA thin film leads us to consider a new model in which Na ions drift and/or become polarized in an amorphous Al_2O_3 matrix.

When the annealing temperature is increased to 1000 °C and annealing time is increased to 15 h, the 90 nm thin film is clearly crystallized. Because of the low softening temperature (850 °C) of ITO glass that we used for devices, we instead used etched Si wafer as the substrate. The XRD pattern of the crystallized thin film is shown in Figure 4. The peaks in the pattern correspond to (102), (107), (108), (206), and (218) planes of the SBA crystal structure. The hump in the XRD pattern is from the amorphous state SiO_2 on the Si wafer substrate. From this experiment, we can conclude that the SBA thin film is not fully crystallized at 830°. It should be reasonable to expect that higher temperature annealing leads to more short-range ordering of SBA film than lower-temperature annealing even though the SBA film is generally amorphous. This difference in the structure will affect the annealing temperature dependence of SBA film capacitance. In an earlier study, it was found that ionic mobility in an oxide glass depended in a complex way on the number and identity of the ions (in that case, Na+ or Ag+) and the effects on the microstructure when the ions were exchanged.[20]

Frequency-Dependent Capacitance of SBA and Al_2O_3. In both SBA and Al_2O_3, the dielectric responses contributed by the Al−O bond should be similar because of the similar polarization ability of Al−O bonds. The difference in dielectric properties of the two materials should instead be caused by the Na+ ions. A more direct way to study the Na+ effect on the capacitance of the SBA and Al_2O_3 material is to measure the AC capacitance of samples with similar thickness under different frequencies. Figure 5 shows the frequency dependent capacitance study of SBA and Al_2O_3. Our data show that the dielectric constant of Al_2O_3 has small frequency dependence, whereas SBA shows much higher capacitance at lower frequency and converges to a value similar to Al_2O_3 samples with increased AC frequency. The capacitance difference between SBA and Al_2O_3 at lower frequency is no doubt from the Na+ movement. We tried three different annealing temperatures, 300 °C, 500 and 700 °C, for SBA thin films, keeping the annealing time at 1 h. We found that the capacitance of SBA thin film depends on the annealing temperature. The trend from Figure 5 is that the capacitance of lower temperature annealed samples is lower than higher temperature annealed samples over the entire frequency range, but the difference is diminished with increasing frequency. Although GISAXS and TEM indicated no long-range order, it is possible that some short-range order develops at the higher temperatures, leading to the ultimate development of crystalline regions at still higher temperatures. The Na+ response to voltage bias could depend on its localized translation within small domains of differing short-range order. The small capacitance dispersion for Al_2O_3 could be from the interface trap density. In an ideal case, the capacitance of Al_2O_3 should be a constant from 1kHz to 1 MHz. Our data shows that capacitance density of Al_2O_3 changed slightly from 123 nF/cm^2 at 1kHz to 112 nF/cm^2 at 1 MHz.

We also found that annealing temperature does change the real ratio of Na ions in the SBA film because Na is one of volatile elements at elevated temperature. From XPS data, we can see that after annealing at 300 °C for one hour, Na:Al ratio(1:12) is only slightly less than the starting ratio (1:11). However, after annealing at 500 and 700 °C for one hour, the Na ratio dropped to 1;20.7 and 1:17.6. The reason that Na ratio for 700 °C annealed sample is higher than 500 °C annealed sample could be just from the measurement error. Even though 300 °C annealed sample has Na almost twice as much as 500 and 700 °C annealed sample, its capacitance is still less than other samples over all frequency range. This experiment demonstrates that both Na ion concentration and crystallinity are contributing factors for the capacitance behavior, again consistent with the earlier study.[20]

The HP 4284 LCR meter measures the impedance of the sample and then calculates capacitance based on the phase angle. A phase angle of −90° means the device is a complete capacitor (current is all capacitive). When the phase angle deviates from

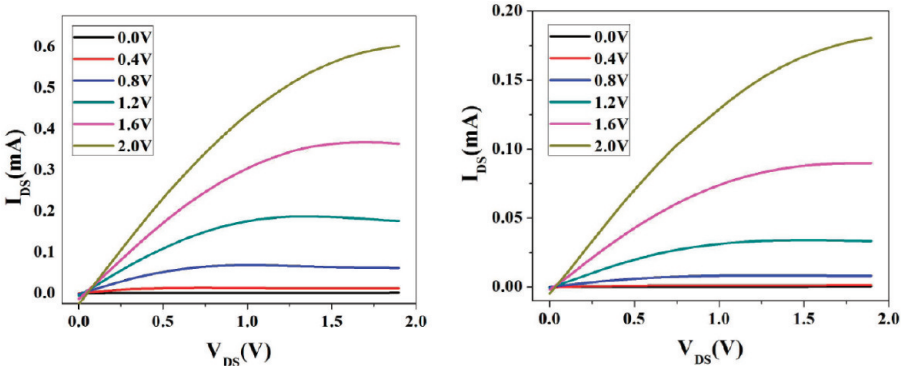

Figure 6. Output curves for (left) fresh ZTO FET and (right) ZTO FET stored in ambient environment for 24 h (W/L ratio = 10).

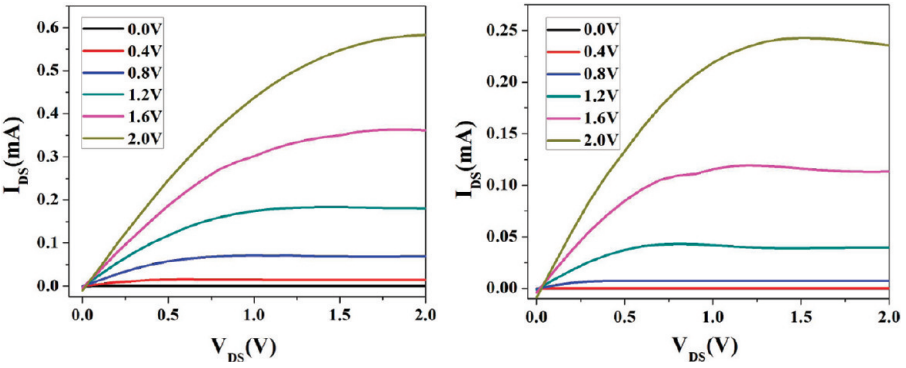

Figure 7. FET output curves after CYTOP coating, ZTO devices stored in ambient environment for 24 h (left) and 72 h (right) (W/L = 10).

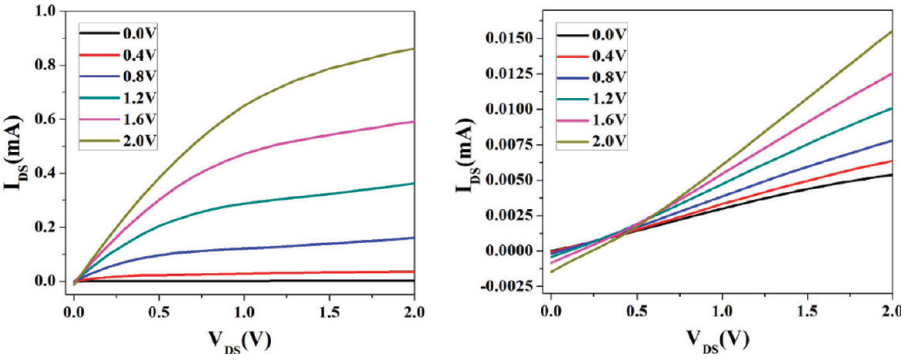

Figure 8. Output curves for SBA-ZTO (left) fresh FET and (right) FET after HMDS coating (W/L = 10).

the −90°, this means that the device not only has a capacitance component but also has a conductance component. The capacitance measurement at lower frequency between 20 Hz and 1000 Hz is not as accurate as at higher frequency because the phase angle is farther from −90°. The typical phase angle at frequency from 20 Hz to 1000 Hz is −75° and above that frequency range the phase angle is about −85°. Therefore, we report capacitance data here from 1kHz to 1 MHz.

There could be three different kinds of states of Na+ ions in the SBA film, depending on the local crystallinity. The first one is that Na+ ions are confined between two spinels and stay in the particular crystallite, of whatever orientation. The second is that the Na+ ions have some conducting path to move from their original crystallite to a certain position where the conducting path ends; the third is that Na+ ions have not grown into an SBA crystal structure at all and are more randomly arranged in an amorphous oxide. The three possible situations will lead to different capacitance in term of not only the magnitude but also the frequency dependence. The second possibility will give larger magnitudes of capacitance and more serious dielectric loss with increasing AC frequency than the first possibility. In the third possibility, the dielectric properties will be a combination of those of Na_2O and Al_2O_3. At this point, we still have no firm basis to eliminate any of these three scenarios as contributing part of the dielectric behavior.

X-ray Photoelectron Spectroscopy (XPS) in a Device Structure. Another experiment that reveals information about the Na+ behavior in SBA is XPS, used to measure the near-

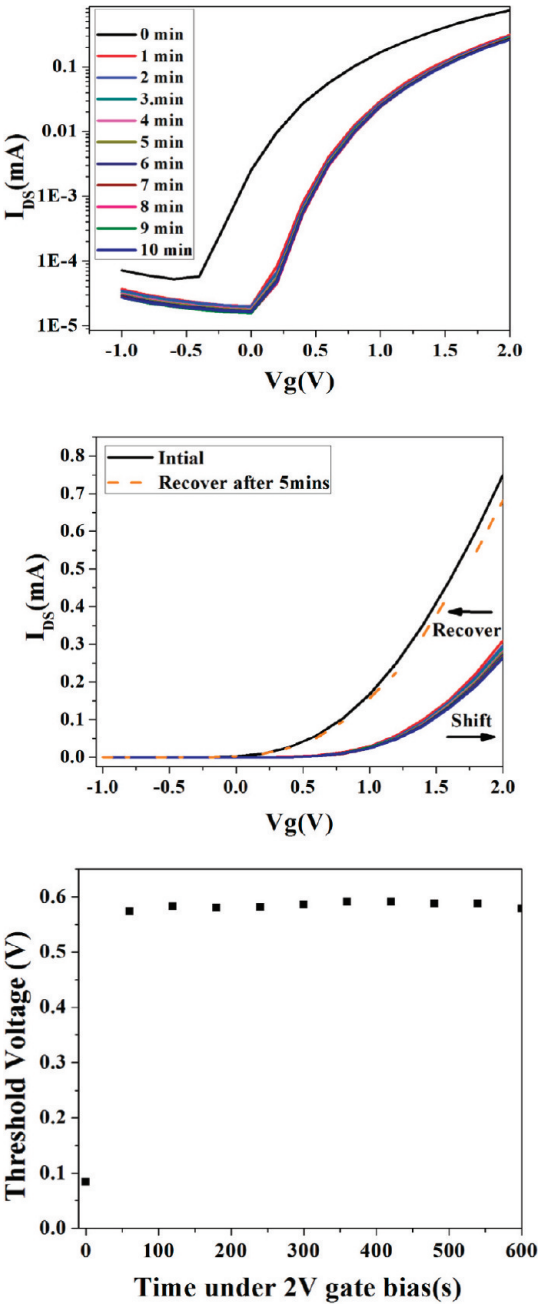

Figure 9. (top) Transfer cureve of the ZTO/SBA under gate bias 2 V (W/L = 10). (middle) Transfer curve recovery after 5 min. (bottom) Threshold voltage shift under gate bias without Cytop coating.

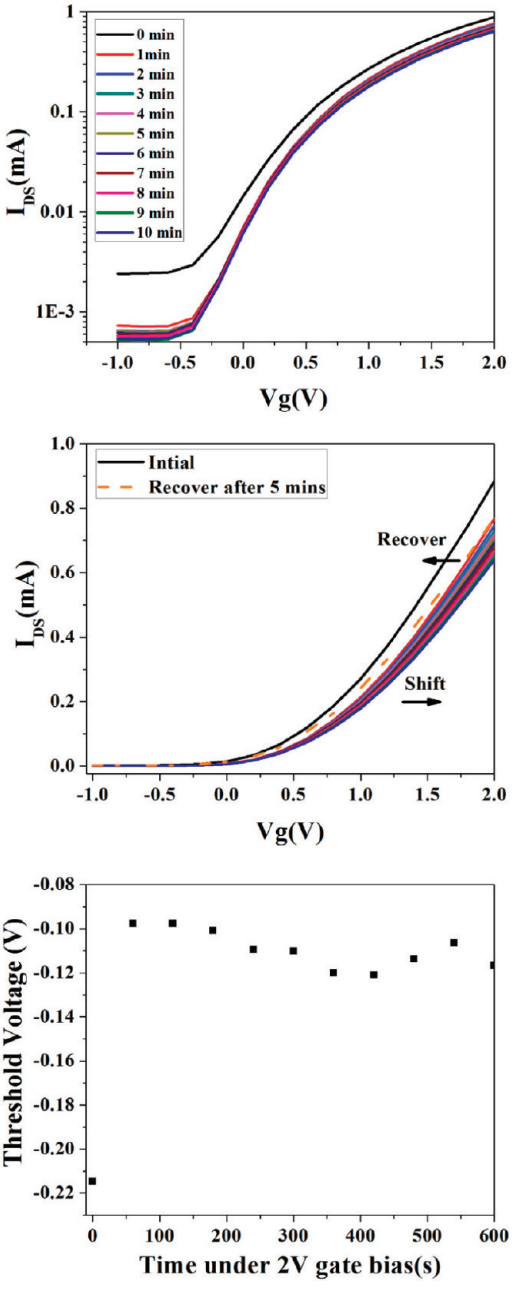

Figure 10. (top) Transfer curve of the ZTO/SBA after coating with Cytop under gate bias 2 V. (middle) Transfer curve recovery after 5 min (W/L = 10). (bottom) Threshold voltage shift under gate bias with Cytop coating.

surface Na atom concentration for SBA samples before and after gate bias. A copper foil was pressed onto the SBA on ITO glass as a top electrode. 2 V bias was applied on the SBA film for 30 min. After applying bias, the control sample and the samples after having applied voltage bias were taken to do XPS. The detected Na concentration for the sample after having applied voltage bias has three times higher Na concentration (atomic ratio Na/Al = 1.2/28.2) than the control samples (atomic ratio Na/Al = 0.4/28.3). Here, the increased Na concentration only reflected the Na trapped on the surface after being moved by the gate bias. After removing the bias, it is possible that some Na ions could have relaxed back to their original position. The conclusion from this experiment is that some small Na+ ion current can be generated globally across the SBA film by gate bias, but is not likely to be responsible for low-voltage or high-frequency dielectric response, nor gate leakage current. However, smaller scale Na+ motions are also likely, and would indeed contribute to the gate dielectric capacitance.

Device Stability Issues in Ambient Environment. Despite the promising properties we have noted for SBA/ZTO FETs, the performance degrades relatively rapidly in the ambient air. Typically, with 24 h, the output current could drop by a factor of 3, as shown in Figure 6. The device degradation could be because of at least two atmospheric components. It is well-known

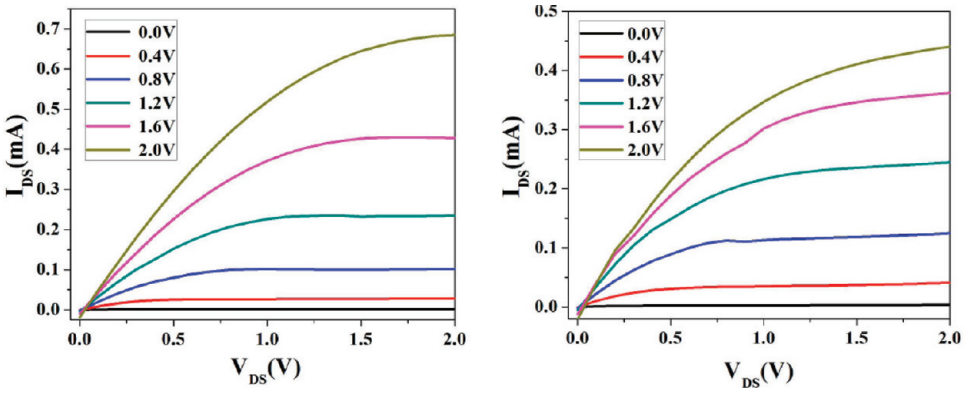

Figure 11. Output curves for ZTO/SBA device under continuous (left) and pulsed (right) gate measurement modes.

that materials like ZTO and IZO (AOS materials) are sensitive to water, oxygen, and even vapors of common solvents such as ethanol and acetone.[21] Physically absorbed O_2 is electrically neutral, but if the O atoms became chemically bonded with defects in an AOS, the O becoming negatively charged will deplete the conduction band, as though it were an acceptor. Water, on the other hand, acts like a donor to generate more free negative carriers. Also, the sensitivity of SBA to moisture has been reported in the past.[22] Physisorbed water in SBA can increase the conductivity of the Na ions. As Na ions become more mobile, the interface charge accumulation could become more significant, causing the degradation of the field driven current. We found that the ZTO/SBA devices stored under regular vacuum show much better stability. Device stored in vacuum did not show degradation in 72 h. This suggests that encapsulating the FETs will prevent degradation. We considered one particular candidate material, CYTOP, for encapsulation. CYTOP is an amorphous fluoropolymer which can be purchased from BELLEX Corporation. As coating layer, it has excellent transparency, electrical insulation, chemical resistance and moisture resistance. CYTOP as a coating layer was spin coated at 5000 rpm for 30s on the completed FET, followed by heat treatment on hot plate at 90 °C for 5 min. We found that after coating CYTOP, the degradation is slowed. As shown in Figure 7 after 24 h, there is no obvious decrease of the current. After 72 h, the current of the device still decreases to about one-third of the original current, about the same amount as the 24 h decrease in the unencapsulated device. Clearly, a more rigorous encapsulation can prevent the degradation much more effectively.

We also tried using hexamethyldisilazane ($(CH_3)_3$ SiNHSi $(CH_3)_3$) (HMDS) coating layers to make the device more hydrophobic. However, we found that HMDS may instead react chemically with the ZTO layer. As shown in Figure 8, the output curve changed significantly including both magnitude of the output current and threshold voltage, implying a strong doping effect arising from the reaction between ZTO and HMDS. Judging from the shape of the output curve, the device after HMDS treatment has threshold voltage shifted significantly in the negative direction, indicating that the HMDS could act as a donor to the ZTO. This experiment indicates that ZTO could potentially be used in sensors for amines.

Threshold Voltage Shift. In practical application, the stability of the threshold voltage is essential for applications which need to be on continuously. For some applications in which the device is not continuously on, such as displays, if this threshold voltage shift is recoverable, then the threshold voltage shift is not of great concern. Amorphous semiconductor oxide FETs generally show threshold voltage shift under gate bias. Under gate bias stress, the ZTO becomes more subject to ambient environment elements, such as water, and more charges accumulate to the interface between gate and semiconductor if there are large defect states on the surface of the gate material.

Our typical transfer curve under 2 V gate bias for SBA/ZTO FETs is shown in Figure 9a. We can see from the threshold voltages plotted in Figure 9c that threshold voltage shifts from 0.09 to 0.57 V in the first 60 s and stays nearly constant in the next 540 s. The absolute value of the threshold voltage shift is not large, only 0.48 V. However, if we consider that the maximum gate voltage is only 2 V, the relative shift is quite large, about 25%. The transfer curve is recoverable; from Figure 9b we can see that after 5 min the current is recovered about 90%. We tried to use 10 nm Al_2O_3 as a capping layer on SBA, but we did not see any improvement.

After coating with CYTOP, previously used as a barrier coating with inorganic oxide devices,[23] we found that the threshold voltage is more stable under gate bias. The transfer curve of ZTO/SBA device with CYTOP coating layer is shown in Figure 10a. It is clearly shown that transfer curve shift is much less than for the device exposed directly to the ambient environment. As plotted in Figure 10b, threshold voltage only shifts about 0.1 V after 60s and then fluctuates around −0.1 V for the remaining 540s. These results suggested that the absorption of the species in the ambient environment is responsible for some of the threshold voltage shift.

Response Time Dependence on the Annealing Temperature. SBA device has a longer response time compared to other conventional dielectric material because of the relatively slow Na+ polarization. This has been demonstrated in the dependence of capacitance on frequency shown in Figure 5. When we use a pulsed-gate-voltage mode (100 ms period and 5 ms width) to measure the output curve of SBA FETs, we found that the maximum output current is reduced by a factor of 3 compared to the normal measurement mode (Figure 11). During the measurement, current is recorded at every 0.1 V increment for 5 ms integration time, during which the semiconductor analyzer integrates the signal and obtains the average value of the current. This integration time has to be equal to the gate pulse time width. After each measurement, there was 100 ms during which time gate voltage was again zero. After 100 ms, the gate voltage reaches the peak again and at the same time source-drain voltage reaches

the next level and then the analyzer starts a 5 ms integration time to record the current data again. Thus, in the pulsed gate measurement mode, the gate is not continuously on and there is 100 ms during which the gate is off. During that time, the Na+ ions could relax back to their original positions. The 5 ms gate width may not be long enough for Na+ ions to be polarized sufficiently to reach the largest capacitance.

CONCLUSION

The dielectric and morphological properties of sol−gel-derived SBA films in FET gates clearly are the result of the incorporation of Na+ ions. The polarization of these ions contributes significantly to capacitance, though longer response times are necessary for full utilization of this capacitance. SBA is also smoother than comparably prepared alumina lacking the Na+ ions, inducing higher mobility in an overlying ZTO film. Gate leakage current is actually lower for the SBA than for plain alumina. Thermal stability and interfacial compatibility of the SBA and ZTO are excellent. While SBA-based FETs lack environmental stability as prepared, simple encapsulation methods improve stability markedly. Future work will include investigation of incorporated ions other than Na+ in order to tune response times and to maximize capacitance and stability.

AUTHOR INFORMATION

Corresponding Author
*E-mail: hekatz@jhu.edu.

ACKNOWLEDGMENT

This work was supported by NSF Division of Materials Research (Grant 1005398, studies of Na+ ion polarization and 0905176, X-ray diffraction) and AFOSR (Grant FA9550-09-1-0259, FET device studies and mobilities). We thank Ken Livi at Electron Microbeam Analytical Facility for the TEM analysis, Dr. Patricia McGuiggan for AFM analysis, and Dr. Kenneth Evans-Lutterodt at Brookhaven national lab for GISAXS analysis. We also thank Drs. William Wilson and Michael Falk for helpful discussions.

REFERENCES

(1) Rogers, J. A.; Bao, Z.; Baldwin, K.; Dodabalapur, A.; Crone, B.; Raju, V. R.; Kuck, V.; Katz, H.; Amundson, K.; Ewing, J.; Drzaic, P. *Proc. Natl. Acad. Sci. U.S.A.* **2001**, *98*, 4835–4840.
(2) Sirringhaus, H.; Kawase, T.; Friend, R. H. *MRS Bull.* **2001**, *26*, 539–543.
(3) Carcia, P. F.; McLean, R. S.; Reilly, M. H.; Nunes, G. *Appl. Phys. Lett.* **2003**, *82*, 1117–1119.
(4) Fortunato, E. M. C.; Barquinha, P. M. C.; Pimentel, A.; Goncalves, A. M. F.; Marques, A. J. S.; Martins, R. F. P.; Pereira, L. M. N. *Appl. Phys. Lett.* **2004**, *85*, 2541–2543.
(5) Fortunato, E. M. C.; Barquinha, P. M. C.; Pimentel, A.; Goncalves, A. M. F.; Marques, A. J. S.; Pereira, L. M. N.; Martins, R. F. P. *Adv. Mater.* **2005**, *17*, 590–594.
(6) Gelinck, G. H.; Huitema, H. E. A.; Van Veenendaal, E.; Cantatore, E.; Schrijnemakers, L.; Van der Putten, J.; Geuns, T. C. T.; Beenhakkers, M.; Giesbers, J. B.; Huisman, B. H.; Meijer, E. J.; Benito, E. M.; Touwslager, F. J.; Marsman, A. W.; Van Rens, B. J. E.; De Leeuw, D. M. *Nat. Mater.* **2004**, *3*, 106–110.
(7) Sekitani, T.; Noguchi, Y.; Zschieschang, U.; Klauk, H.; Someya, T. *Proc. Natl. Acad. Sci. U.S.A.* **2008**, *105*, 4976–4980.
(8) Yabuta, H.; Sano, M.; Abe, K.; Aiba, T.; Den, T.; Kumomi, H.; Nomura, K.; Kamiya, T.; Hosono, H. *Appl. Phys. Lett.* **2006**, *89*, 112123.
(9) Robertson, J. *Eur. Phys. J.—Appl. Phys.* **2004**, *28*, 265–291.
(10) Peacock, P. W.; Xiong, K.; Tse, K.; Robertson, J. *Phys. Rev. B: Condens. Matter Mater. Phys.* **2006**, *73*, 12.
(11) Pal, B. N.; Dhar, B. M.; See, K. C.; Katz, H. E. *Nat. Mater.* **2009**, *8*, 898–903.
(12) Yoldas, B. E. *J. Mater. Sci.* **1975**, *10*, 1856–1860.
(13) Kim, S.; Nah, J.; Jo, I.; Shahrjerdi, D.; Colombo, L.; Yao, Z.; Tutuc, E.; Banerjee, S. K. *Appl. Phys. Lett.* **2009**, *94*, 3.
(14) Kalb, W.; Lang, P.; Mottaghi, M.; Aubin, H.; Horowitz, G.; Wuttig, M. *Synth. Met.* **2004**, *146*, 279–282.
(15) E.C.Subbarao, A. K. R. *Mater. Res. Bull.* **1975**, *10*, 583–590.
(16) Bong, H.; Lee, W. H.; Lee, D. Y.; Kim, B. J.; Cho, J. H.; Cho, K. *Appl. Phys. Lett.* **2010**, *96*, 192115.
(17) Kim, M. G.; Kim, H. S.; Ha, Y. G.; He, J. Q.; Kanatzidis, M. G.; Facchetti, A.; Marks, T. J. *J. Am. Chem. Soc.* **2010**, *132*, 10352–10364.
(18) Bose, A.; Pal, B. N.; Datta, A.; Chakravorty, D. *J. Non-Cryst. Solids* **2009**, *355*, 1448–1452.
(19) Chen, Y. C.; Ai, X.; Huang, C. Z.; Wang, B. Y. *Mater. Sci. Eng., A* **2000**, *288*, 19–25.
(20) Srivastava, A. K.; Roy, S.; Chakravorty, D. *J. Mater. Sci.* **1990**, *25*, 3236–3240.
(21) Conley, J. F. *IEEE Trans. Device Mater. Reliab.* **2010**, *10*, 460−475.
(22) Kaneda, T.; Bates, J. B.; Wang, J. C.; Engstrom, H. *MRS Bull.* **1979**, *14* (8), 1053–1056.
(23) Banger, K. K.; Yamashita, Y.; Mori, K.; Peterson, R. L.; Leedham, T.; Rickard, J.; Sirringhaus, H. *Nat. Mater.* **2011**, *10*, 45–50.